

Operating principles and detection characteristics of the Visible and Near-Infrared Imaging Spectrometer in the Chang'e-3 *

Zhi-Ping He¹, Bin-Yong Wang¹, Gang Lü¹, Chun-Lai Li¹, Li-Yin Yuan¹, Rui Xu¹,
Bin Liu², Kai Chen¹ and Jian-Yu Wang¹

¹ Key Laboratory of Space Active Opto-Electronics Technology, Shanghai Institute of Technical Physics, Chinese Academy of Sciences, Shanghai 200083, China; jywang@mail.sitp.ac.cn

² The Science and Application Center for Moon and Deep Space Exploration, National Astronomical Observatories, Chinese Academy of Sciences, Beijing 100012, China

Received 2014 July 18; accepted 2014 October 14

Abstract The Visible and Near-Infrared Imaging Spectrometer (VNIS), using two acousto-optic tunable filters as dispersive components, consists of a VIS/NIR imaging spectrometer (0.45–0.95 μm), a shortwave IR spectrometer (0.9–2.4 μm) and a calibration unit with dust-proofing functionality. The VNIS was utilized to detect the spectrum of the lunar surface and achieve in-orbit calibration, which satisfied the requirements for scientific detection. Mounted at the front of the Yutu rover, lunar objects that are detected with the VNIS with a 45° visual angle to obtain spectra and geometrical data in order to analyze the mineral composition of the lunar surface. After landing successfully on the Moon, the VNIS performed several explorations and calibrations, and obtained several spectral images and spectral reflectance curves of the lunar soil in the region of Mare Imbrium. This paper describes the working principle and detection characteristics of the VNIS and provides a reference for data processing and scientific applications.

Key words: space vehicles: instruments — instrumentation: spectrographs — Moon — techniques: spectroscopic

1 INTRODUCTION

The Visual and Near-infrared Imaging Spectrometer (VNIS) is one of the main scientific payloads on the Yutu lunar rover that is part of the Chang'e-3 project. It uses two acousto-optic tunable filters (AOTFs) as dispersive components and consists of a VIS/NIR imaging spectrometer (0.45–0.95 μm), a shortwave infrared (SWIR) spectrometer (0.9–2.4 μm) and a calibration module that is protected from dust. The VNIS is mounted at the front of the Yutu rover to obtain spectra and geometric data about objects on the lunar surface. The rover and VNIS are shown in Figure 1.

The Chang'e-3 spacecraft consists of the lander and the Yutu lunar rover, each of which carries appropriate scientific payloads. After soft landing on the Moon, Chang'e-3 completed a lunar scientific exploration mission. The scientific exploration mission of Chang'e-3 (Ye & Peng 2006;

* Supported by the National Natural Science Foundation of China.

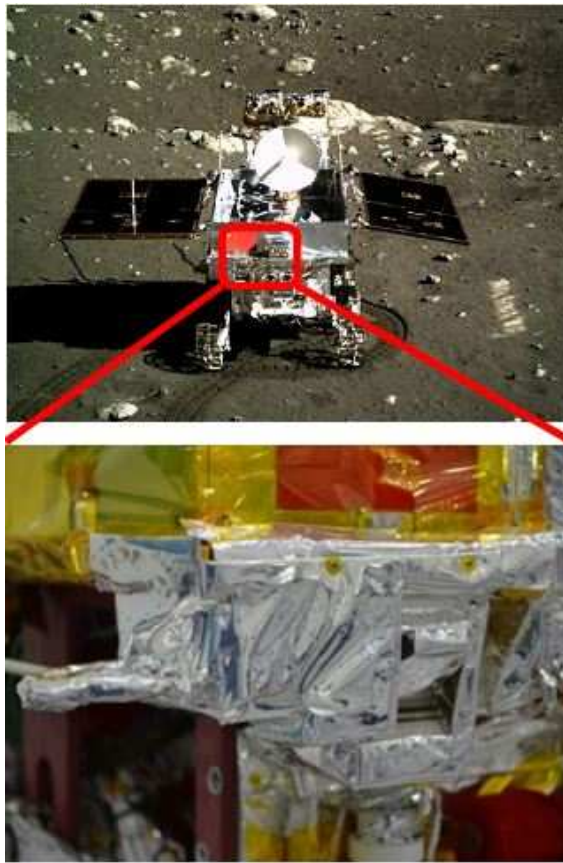


Fig. 1 Rover (*upper*) and VNIS (*lower*).

Dai et al. 2014; Ouyang 2004) has several objectives: (1) a survey of the lunar surface topography and geological structure (Ip et al. 2014), (2) exploration of mineral compositions on the lunar surface and available resources, (3) detection of the plasma layer associated with Earth and conducting Moon-based ultraviolet astronomical observations. The VNIS was mostly involved with the second objective. This paper describes the working principle and detection characteristics of the VNIS and provides a reference for data processing and applications.

In this article, Section 2 gives scientific objectives of VNIS. Then from Section 3 to 4, the major functional, performance, composition and operation principle are provided. After that, Section 5 mainly presents characteristics such as geometric, spectral and radiance of VNIS. Section 6 shows the primary detection results of VNIS on 2013 Dec. 23, when the VNIS was booted for the first time. Section 7 gives conclusions.

2 SCIENTIFIC OBJECTIVES

Morphological measurement and spectral measurement are the two major methods of analyzing rock structures and compositions. Imaging spectrometers can obtain both spectra and images at the same time and are widely used in remote sensing of Earth and space. Minerals such as pyroxene, plagioclase, olivine and ilmenite, in different sizes and shapes, constitute most rocks on the lunar surface (Liu et al. 2013). They have distinctive spectral characteristics in the VIS/NIR and SWIR wavebands that can be used for identification. The specific scientific objectives and mission of the

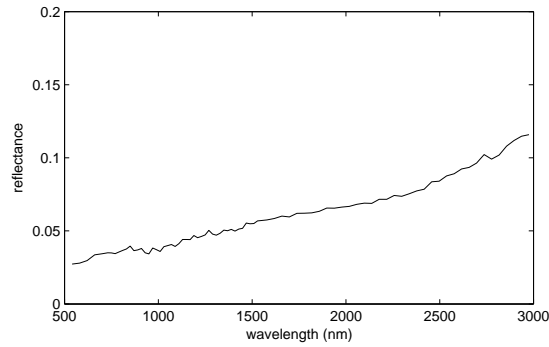


Fig. 2 Spectral reflectance curve of the Chang'e-3 landing region as detected by M^3 (Courtesy of Brown University and NASA).

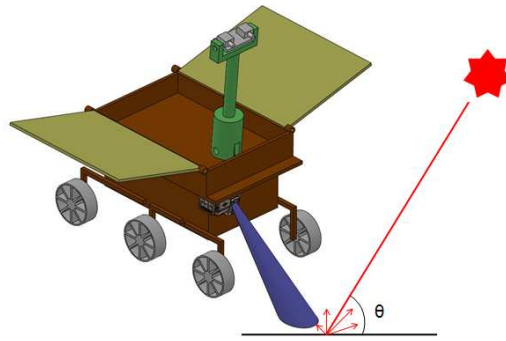


Fig. 3 Schematic of detection by VNIS.

VNIS are to obtain the spectra and geometric data for objects on the lunar surface, which are used for: (1) determining the mineral composition and analyzing the distribution of materials on the lunar surface over the roving area and (2) a comprehensive study of energy and mineral resources over the roving area. The spectral reflectance curve for the Chang'e-3 landing region, as detected by the U.S. hyperspectral camera Moon Mineralogy Mapper (M^3) carried on India's Chandrayaan-1, is shown in Figure 2.

Changes in the solar elevation angle and spectral reflectance of the object strongly affect the properties of spectral data detected by the VNIS. As one of the scientific payload on the Yutu rover, the VNIS detected the material composition using the sunlight reflectance spectrum taken at a 45° visual angle, as shown in Figure 3. The range of spectral radiance for the detected objects determines the dynamic range of the instruments used for detection, and the VNIS was expected to explore objects at solar elevation angles of 15° – 45° and reflectances of objects on the lunar surface of 5%–98% (objects on the lunar surface and the diffusion panel of the calibration unit).

3 FUNCTIONALITY AND PERFORMANCE

The VNIS has the following functions: (1) obtain spectral image data on specified objects in the visible and NIR (0.45 – $0.95 \mu\text{m}$) and spectral data on specified objects in the SWIR (0.9 – $2.4 \mu\text{m}$), (2) obtain reflectance spectral images in the visible and NIR and reflectance spectra in the SWIR, (3)

Table 1 Major Technical Specification

Description	Specification
Spectral range (nm)	450–950 (VIS/NIR), 900–2400 (SWIR)
Spectral resolution (nm)	2–7 (VIS/NIR), 3–12 (SWIR)
FOV (°)	8.5 × 8.5 (VIS/NIR), Φ3.6 (SWIR)
Effective pixel count	256 × 256 (VIS/NIR), 1 (SWIR)
Quantized values (bit)	10 (VIS/NIR), 16 (SWIR)
SNR (dB)	> 31 (VIS/NIR), > 32 (SWIR)
Power consumption (W)	19.8
Weight (kg)	4.7 (probe) and 0.7 (electrical component in RECB)

perform on-orbit calibration and (4) provide dust-proofing and insulation. After the rover separated from the lander, the VNIS began operation within an appropriate time after reaching a designated location. Table 1 shows the main performance indicators of the VNIS. The VNIS has two operating modes: detection mode and calibration mode (He et al. 2011, 2014a,b).

Detection mode: The VNIS obtains scientific data about object on the lunar surface. The default spectral sampling interval is 5 nm, and the total number of bands that are sampled is 400. In addition, the VIS/NIR and SWIR channels both need to collect 20 extra dark frames for data processing.

Calibration mode: Using solar spectral irradiation (Gueymard 2004) as the calibration source, the diffusion panel that is part of the calibration unit is set to a horizontal position to calibrate the device. The workflow of the calibration mode is exactly the same as that of the detection mode.

4 OPERATING PRINCIPLES AND COMPOSITION OF VNIS

During operation of VNIS, single-band spectral or imaging information about objects on the lunar surface passes through the AOTF (a set of narrow-band filters that are rapidly switched by altering the input radio frequency (RF) that can be controlled by an electrical signal), forming quasi-monochromatic light of a certain wavelength and converging on the detector. The VNIS can realize flexible and rapid wavelength selection by altering the driving frequency exerted on the AOTF, so we can acquire spectral or imaging data in all the available wavebands. Furthermore, the VNIS uses a lightweight ultrasonic motor to adjust the calibration unit.

The VNIS consists of the probe and one electronic section of the Remote Electrical Control Box (RECB). The electronic section forms the scientific payload of the RECB containing the RF module of VNIS, ground penetrating radar, and an alpha particle X-ray spectrometer (Dai et al. 2014). The probe consists of pre-optical components (including the calibration and dust-proofing components and image-forming and collimating lenses for the VIS/NIR and SWIR channels), the AOTFs, the convergent lenses, the detector components, the ultrasonic motor and its drive, and the main control circuit. Figure 4 shows a schematic diagram of the VNIS systems.

The VNIS probe is installed outside the vehicle, whereas the RECB is installed in the cabin. The probe and RECB are connected by cables for power supply and communication. The probe and a schematic illustration of its installation are shown in Figure 5.

The VNIS detects objects on the lunar surface from a height of 0.69 m above the lunar surface at a 45° visual angle, as shown in Figure 6. The AOTF is a light-splitting component based on an acousto-optic effect and made by a solid crystalline material. On the basis of the acoustic-optic effect, when an acoustic wave propagates in an anisotropic medium, the AOTF will cause Bragg diffraction of the light, which enables it to select the wavelength. The light-splitting principle and actual equipment are shown in Figure 7. Single-band spectral and imaging information about objects on the lunar surface pass through the AOTF and are photoelectrically transformed by the detector, forming quasi-monochromatic light of a certain wavelength. The VNIS can select the wavelength of monochromatic light by altering the driving frequency exerted on the AOTF, so we can acquire spectral and imaging data at different wavelengths and detect in all the available wavebands.

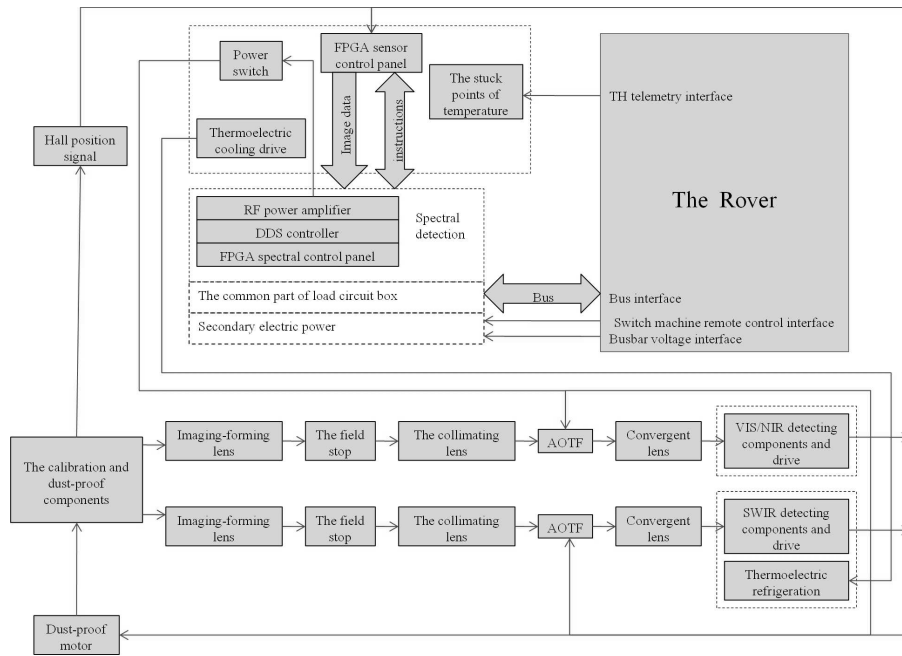


Fig. 4 Schematic diagram of the VNIS system.

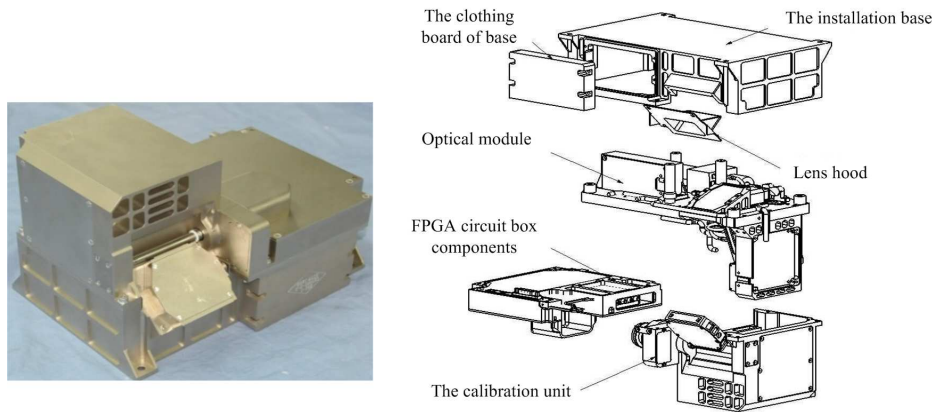


Fig. 5 VNIS probe and schematic illustration of its installation (He et al. 2011, 2014a,b).

The VNIS uses a lightweight ultrasonic motor to drive the calibration panel to achieve on-orbit calibration, dust-proofing and detection and to switch between the three modes (Fig. 8). The inner surface of the calibration unit is the diffusion panel, which is located near the light entrance. When the spectrometer is operated in detection mode, the calibration unit can be completely open at a 55° angle with respect to the mounting plane, which does not affect entrance of the light. When the spectrometer is operated in calibration mode, the solar spectral irradiance is used as a calibration source, and the diffusion panel of the calibration unit is positioned parallel to the mounting plane to obtain calibration data (He et al. 2014b; Xu et al. 2014b). When it is not working, the calibration unit

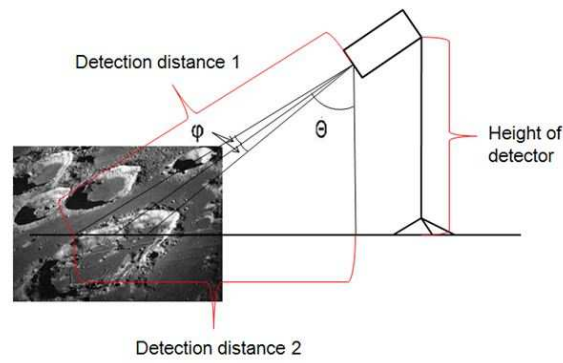


Fig. 6 Schematic illustration of VNIS detection.

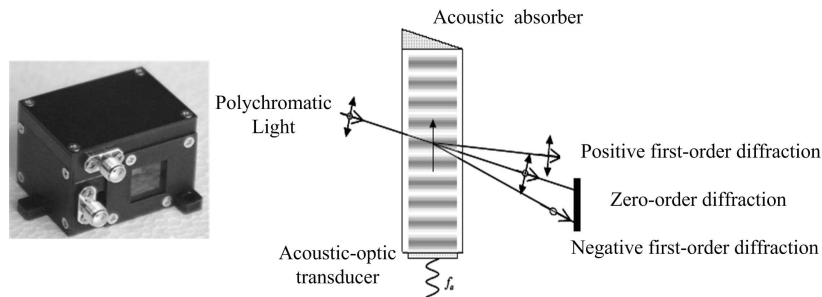


Fig. 7 AOTF and schematic illustration (Gupta 2005) of the light splitting operation.

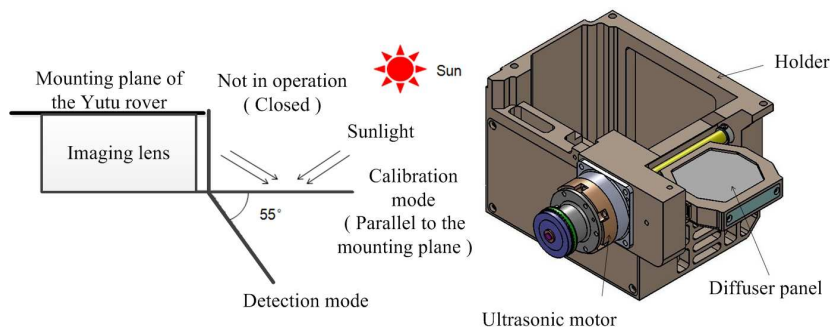


Fig. 8 Detection, calibration and dust-proofing scheme of VNIS.

can be closed up within the framework to prevent damage to the spectrometer from dust and other pollution and also to provide good thermal insulation.

The diffusion panel (Xu et al. 2014b) that is part of VNIS uses Teflon material, whose directional-hemispherical reflectance (DHR), uniform reflectance and bidirectional reflectance factor (BRF) were accurately measured, as shown in Figure 9. The DHR measurement can be traced to the National Institute of Metrology (NIM), China. It is based on a standard diffusion screen that was tested by the NIM and uses an integral sphere system with a double light path to set the standard;

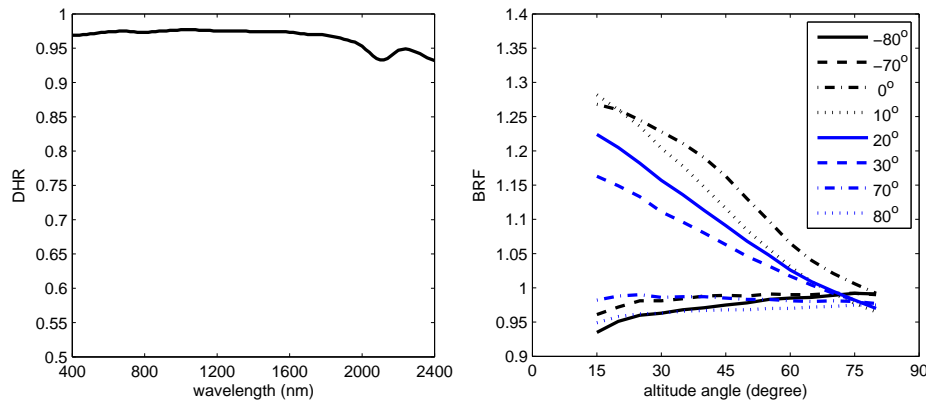


Fig.9 DHR of the calibration unit (*left*) and BRF of calibration unit in different azimuth conditions @600 nm (*right*).

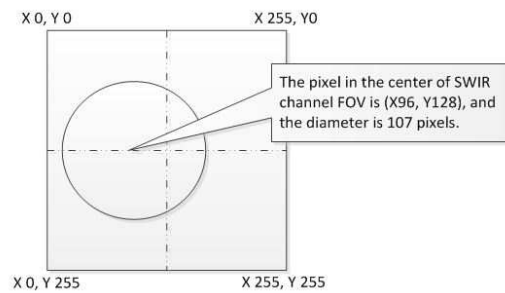


Fig.10 Geometrical relationship in VNIS detection.

the measurement error is 1.3%. The BRF was measured by comparing the radiance between the diffusion panel of the calibration unit and the standard diffuse reflection plate. The reference board is provided by the Key Laboratory of Optical Calibration of Anhui Institute of Optics and Fine Mechanics and can be traced to the hemispherical standard reflectance of the NIM. The uncertainty in the final measurement is less than 2.5%.

5 MAIN DETECTION AND CALIBRATION CHARACTERISTICS

The VNIS can obtain an image and a spectrum. It can obtain a spectral image in the VIS/NIR band and spectral data in the SWIR band simultaneously. The main characteristics of the VNIS are its geometrical detection characteristics, spectral characteristics and radiometric response characteristics.

5.1 Geometric Detection Characteristics

The VNIS is used to detect objects on the lunar surface parallel to the optical axis at a distance of 18 mm. The fields of view (FOVs) in the VIS/NIR and SWIR are $8.5^\circ \times 8.5^\circ$ and $\Phi 3.6^\circ$, respectively. The geometrical characteristics of imaging in the VIS/NIR band and spectral detection in the SWIR, obtained by testing and calibration on the ground, are shown in Figure 10 (He et al. 2014a,b).

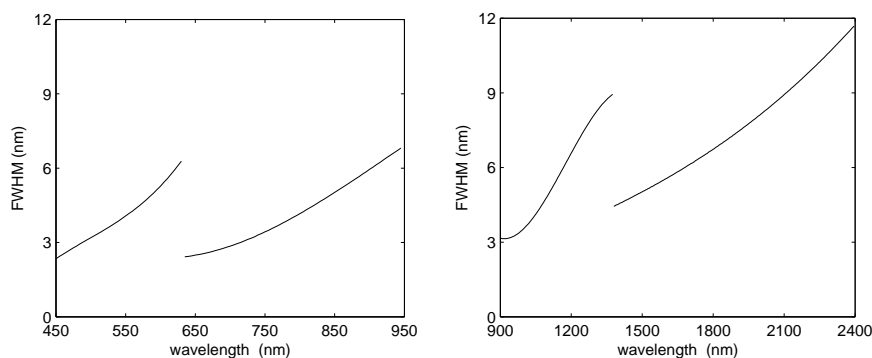


Fig. 11 Spectral resolution of VNIS (*Left*: VIS/NIR channel; *Right*: SWIR channel).

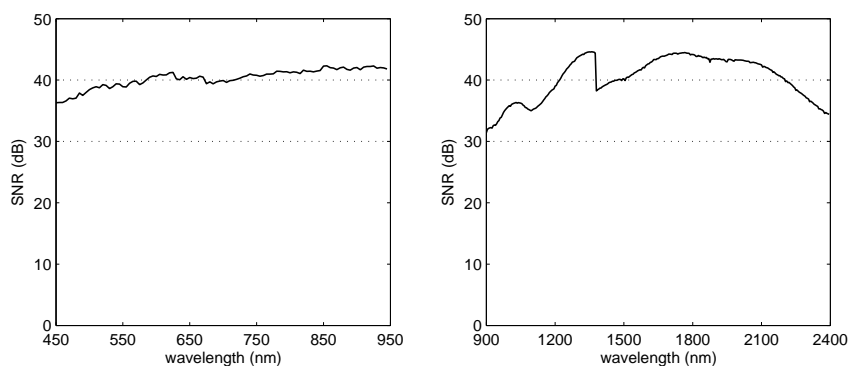


Fig. 12 Lunar surface condition equivalent SNR of VNIS (*Left*: VIS/NIR channel; *Right*: SWIR channel).

5.2 Spectral Characteristics

The spectral range and resolution of the VNIS are key performance indicators for achieving the scientific objectives and are directly related to the instrument's ability to identify the spectrum. After calibration on the ground and confirmation of the calibration, the spectral ranges of the VNIS are 449–950 nm in the VIS/NIR band and 899–2402 nm in the SWIR band. The spectral resolutions are 2–7 nm in the VIS/NIR band and 3–12 nm in the SWIR band, as shown in Figure 11.

5.3 Radiometric Response Characteristics

The signal-to-noise ratio (SNR) changes with the input signal and is an important indicator of the radiometric response characteristics of the VNIS. When the noise is fixed, the SNR is obviously higher if the amplitude of the input signal is higher. The SNR is greater than 30 dB in the VIS/NIR band when the albedo is 0.09 and the solar elevation angle is 45° ; when the albedo is 0.09 and the solar elevation angle is 15° , the SNR is greater than 30 dB in the SWIR band. The SNR of the VNIS was tested and analyzed by ground radiometric calibration. First, by calculating the proportionality relationship between the lunar surface reflection radiance and the energy level of the integrating sphere at different solar elevation angles, we ensured that the energy level is sufficient for calibration at different wavelengths in the spectral response range to adapt to changes in radiance on the lunar

surface during orbital detection. Then, we measured the quantitative relationship between the VNIS's input signal radiance and the spectral image cube's response for each element, which was based on a laboratory radiometric standard source. At the same time, we established an information delivery model for spectral data and an inversion model of the radiance, which created the radiation correction parameters, and obtained the SNR by calculation, as shown in Figure 12.

6 CHARACTERISTICS OF DATA AND PRIMARY DETECTION RESULTS

6.1 Characteristics of the Scientific Data

With a spectral sampling interval of 5 nm, the VNIS was programmed to automatically scan detected the lunar surface, and it sequentially sampled 100 frames of spectral images in the VIS/NIR band and 300 frames of spectral data in the SWIR band. In addition, an extra 20 dark current frames were obtained for subsequent data processing of each band. The flowchart is shown in Figure 13.

The images and spectral data obtained in detection and calibration modes were the original light response signals, which should be used in subsequent data preprocessing and scientific analysis. The data preprocessing (Tan et al. 2014; Liu et al. 2014) that was applied to the raw data included dark current reduction and temperature, radiometric, and geometric corrections. To eliminate the effects of data preprocessing on the original detection data and convert from dimensionless raw data to the spectral radiance values of actual objects on the lunar surface, we used not only a processing algorithm and the real-time detection of the dark current data in detection and calibration modes, but also a temperature correction algorithm (Xu et al. 2014a) determined by ground calibration experiments and radiometric calibration data. The scientific data processing mainly included operations for reflectivity inversion and luminosity correction; the goal was to obtain real scientific data for the lunar surface that had physical meaning. The data in each frame were recorded by the VNIS in orbit, which contained scientific data and the corresponding engineering parameters, which were obtained through the data transmission channel; this included data in detection and calibration modes. The sizes of images in the VIS/NIR band and spectral data in the SWIR are $256 \times 256 \times 16$ bits and 3×16 bits, respectively.

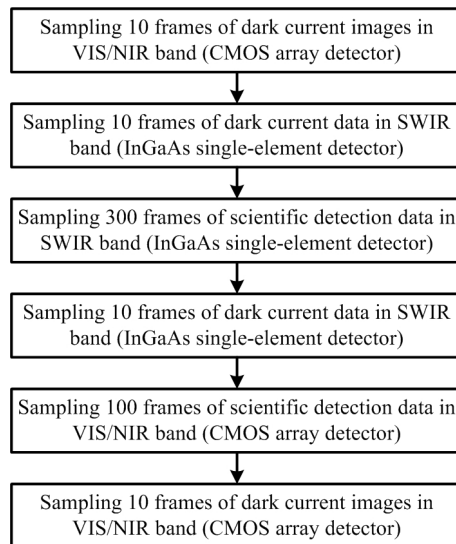


Fig. 13 Flowchart of the detection process.

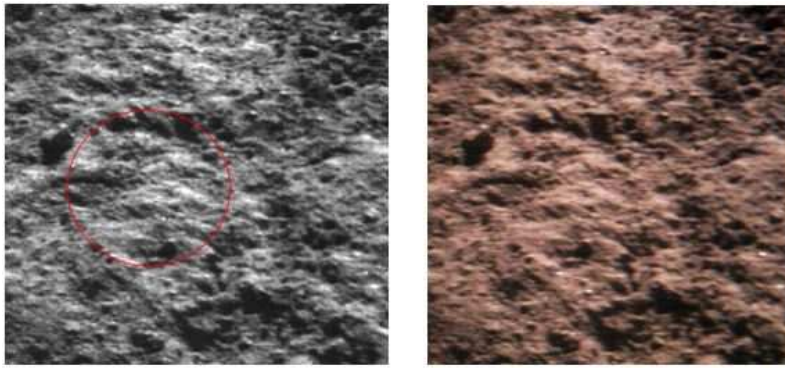


Fig. 14 Primary results of VNIS (1): monochrome picture (630 nm, *left*) and false color picture (500, 550 and 645 nm, *right*).

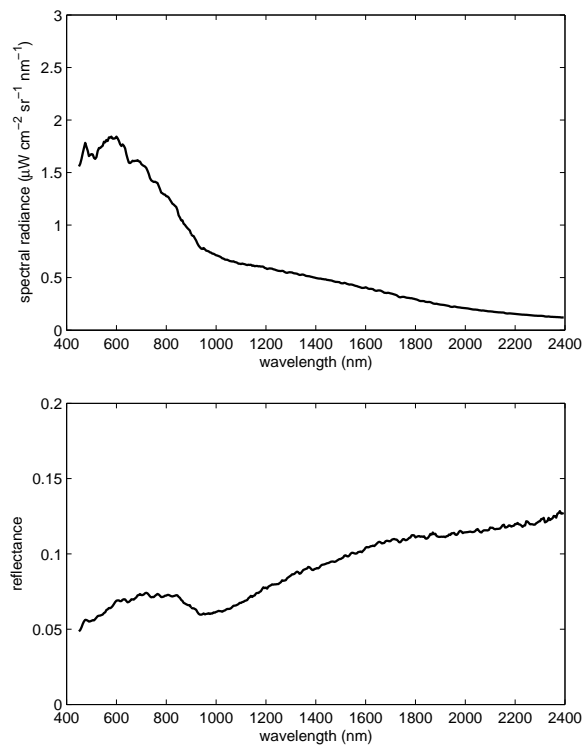


Fig. 15 Primary results of VNIS (2): spectral radiance curve (*upper*) and spectral reflectance curve (*lower*).

6.2 Primary Detection Results

The VNIS acquired several spectral images and data from different regions of the lunar soil and detected objects since it began operation on 2013 Dec. 23. Figures 14 and 15 show the primary results from the VNIS. Figure 14 shows spectral images of lunar soil, and Figure 15 shows the spectral

radiance curve (upper) and spectral reflectance curve (lower). A preliminary analysis revealed that the spectrum exhibits typical characteristic absorption peaks of pyroxene and olivine.

7 CONCLUSIONS

As the main scientific payload of the Chang'e-3 rover, the VNIS was developed to obtain spectra and geometric data to meet the scientific goals for obtaining data on the composition of lunar surface material and for resource exploration. The VNIS completed a ground test, calibration and environmental simulation test before it was booted up. The VNIS performed several lunar detections and calibrations after it booted successfully on 2013 Dec. 23. It obtained certain spectral images and data, and provided a reference for scientific applications.

Acknowledgements This paper is supported by the Chinese lunar exploration program's special funds of the second phase and the National Natural Science Foundation of China (Grant No. 21105109). We thank the Science and Application Center of the Moon and Deep Space Exploration of the Chinese Academy of Sciences for the ground test and data preprocessing. We also thank the National Space Science Center of the Chinese Academy of Sciences for related work in the aspects of development and test of the instruments.

References

- Dai, S. W., Jia, Y. Z., Zhang, B. M., et al. 2014, *Science China: Technological Sciences*, 44, 361
- Gueymard, C. A. 2004, *Solar Energy*, 76, 423
- Gupta, N. 2005, in *Society of Photo-Optical Instrumentation Engineers (SPIE) Conference Series*, 5953, Acousto-optics and Photoacoustics, ed. A. Sliwinski, R. Reibold, & V. B. Voloshinov, 190
- He, Z., Shu, R., & Wang, J. 2011, *Proc. SPIE 8196, International Symposium on Photoelectronic Detection and Imaging 2011: Space Exploration Technologies and Applications*, 8196, 819625
- He, Z. P., Wang, B. Y., Lv, G., et al. 2014a, *Review of Scientific Instruments*, 85, 083104
- He, Z., Xu, R., Wang, B., et al. 2014b, *Proc. SPIE Asia-Pacific Remote Sensing 2014, the Multispectral Hyperspectral Ultraspectral Remote Sens. Technol. Techniques Appl. V conference*, 9263-13
- Ip, W.-H., Yan, J., Li, C.-L., & Ouyang, Z.-Y., 2014, *RAA (Research in Astronomy and Astrophysics)*, 14, 1511
- Liu, B., Liu, J.-Z., Zhang, G.-L., et al. 2013, *RAA (Research in Astronomy and Astrophysics)*, 13, 862
- Liu, B., Li, C. L., Zhang, G. L., et al. 2014, *RAA (Research in Astronomy and Astrophysics)*, 14, 1578
- Ouyang, Z. 2004, *Advances in Earth Science*, 19, 355
- Tan, X., Liu, J., Li, C., et al. 2014, *RAA (Research in Astronomy and Astrophysics)*, 14, 1682
- Xu, R., He, Z., Chen, K., et al. 2014a, *Journal of Infrared and Millimeter Waves*, 33, 327
- Xu, R., Lv, G., Ma, Y., & Wang, J. 2014b, *Proc. SPIE Asia-Pacific Remote Sensing 2014, the Multispectral Hyperspectral Ultraspectral Remote Sens. Technol. Techniques Appl. V Conference*, 9263-43
- Ye, P. J., & Peng, J. 2006, *Engineering Sciences*, 8, 1